Available online at www.sciencedirect.com
SCIENCE DIRECT
Journal of Molecular Catalysis A: Chemical 255 (2006) 53–61
JOURNAL OF MOLECULAR CATALYSIS A: CHEMICAL
www.elsevier.com/locate/molcata

Characterization, adsorption and photocatalytic activity of vanadium-doped TiO_2 and sulfated TiO_2 (rutile) catalysts: Degradation of methylene blue dye

Mohamed Mokhtar Mohamed [a,*], Mater M. Al-Esaimi [b]

[a] *Faculty of Science, Chemistry Department, Benha University, Benha, Egypt*
[b] *Department of Chemistry, Faculty of Applied Sciences, Umm Al-Qura University, Makkah Al-Mukarramah P.O. Box 4496, Saudi Arabia*

Received 8 March 2006; received in revised form 28 March 2006; accepted 29 March 2006
Available online 6 May 2006

Abstract

Sulfated (5 wt.%) TiO_2 and non-sulfated TiO_2 (rutile) modified by NH_4VO_3 using incipient wetness impregnation technique to achieve a loading of 2 wt.% V_2O_5 were thoroughly characterized by means of X-ray powder diffraction (XRD), Fourier-transform infrared spectroscopy (FT-IR), UV–vis absorption spectroscopy, N_2 sorptiometry, particle size analyzer and pyridine-FT-IR that was used to investigate the acidity of the samples. Degradation of methylene blue (MB) dye was tested for the effectiveness of the samples. The results revealed that MB degradation was highly improved with V supported on TiO_2–SO_4 and showed a conversion comprises of 98% after UV irradiation (emitting at 400 nm) for 70 min exceeding that of SO_4 free TiO_2 sample (78%) obtained at the same period of illumination. This was due to the large surface area (345 $m^2\ g^{-1}$), small crystallites size, reduced band-gap energy and presence of basic sites namely O_2^- and OH^- moieties those take part in the reaction as additional oxidizing agents. The photocatalytic degradation of MB was found to follow first order rate kinetics. More information on the activity, surface texturing, kinetics and TOC removal were well evaluated, compared and discussed for all samples.

Keywords: Acidity; Kinetics; Photodegradation; Methylene blue dye; Sulfated titania; Texturing

1. Introduction

It has been documented that some azo dyes are toxic and even mutagenic to living organisms in aquatic environment [1,2]. The release of these colored wastewaters in the ecosystem is a dramatic source of aesthetic pollution, eutrophication and perturbation degradation. Therefore, decolorization of dye effluents using new technologies with more efficiency and less energy used has acquired increasing attention. In recent years, efforts have been devoted to the study of photochemical processes using semiconductor oxides, such as TiO_2, CdS, or ZnO, in heterogeneous system [3,4].

As TiO_2 is illuminated by light with wavelength below 380 nm, the photons excite valence band electrons across the band gap into the conduction band, leaving holes behind in the valence band. The holes in TiO_2 react with water molecules or hydroxide ions and then produce hydroxyl radicals [5]. TiO_2 anatase is usually more active than rutile, but the actual efficiency of titanium dioxide depends not only on its phase composition, but also on the particle size, morphology, and porosity. Anatase higher activity is usually attributed to its larger specific surface area [6]. Poor adsorption and low surface area properties lead to great limitations in exploiting the photocatalyst to the best of its photoefficiency. On the other hand, lower photocatalytic activity of the rutile sample is probably related to the lower specific surface area due to calcination at temperatures above 950 °C. However, for application as a photocatalyst under sunlight, rutile has the potential to absorb solar energy sufficiently more than anatase [7], thus improving the photocatalytic efficiency of rutile is desirable.

Several attempts have been made to improve the photoefficiency of anatase titania by adding adsorbents like silica, alumina, zeolites, clays, and active carbon [8–13]. This is expected to induce synergism because of the adsorption properties of the adsorbents with respect to organic molecules. Conversely, scarce attention has been paid for rutile modification. Thus, it

* Corresponding author. Present address: Department of Chemistry, Faculty of Applied Sciences, Umm Al-Qura University, Makkah Al-Mukarramah, P.O. Box 3605 unit 71, Saudi Arabia. Tel.: +966 0500969808.
E-mail address: mohmok2000@yahoo.com (M.M. Mohamed).

1381-1169/$ – see front matter © 2006 Elsevier B.V. All rights reserved.
doi:10.1016/j.molcata.2006.03.071

was the thought of improving the photocatalytic efficiency of rutile through the advantages of utilizing its absorption capabilities for solar energy.

Using the acidic catalysts in the modern chemical industries or for the production of fine chemicals have drawn much attention recently [14,15]. The liquid acid like H_2SO_4 was often used; however, there were several disadvantages like the corrosion of equipment and environmental pollution. There were more and more works for developing efficient solid acids for the replacement of H_2SO_4 application [16–18], leading to cleaner processes. Since the primary work of Arata and Hino in 1979 [19], the super acids by sulfated metal oxides have gained more attention from investigators. This is because of the thermal stability and acidity gained after sulfation process [20]. In addition, doping with anionic species such as sulphur in TiO_2 led to enhanced photocatalytic activity [21,22] rather than using transition metal doping that indicated no appreciable change in band gap energy of TiO_2 [23,24] as anionic species did.

Thus, in the present paper, we will focus on improving photocatalytic efficiencies of rutile by sulfate ions for the purpose of decomposing methylene blue dye. In addition, the activity of vanadium incorporated inside titania either sulfated or not will also be examined. The textural properties and the crystalline structure of the materials were studied by using BET, X-ray powder diffraction (XRD), particle size analyzer, UV–vis and FT-IR techniques. The acidity was measured by using in situ FT-IR of pyridine adsorption.

The reason for choosing methylene blue dye is due to its wider applications that include coloring paper, temporary hair colorant, dyeing cottons, wools and coating for paper stock and thus acute exposure to methylene blue (MB) will cause health problems such as increased heart rate, vomiting, shock, Heinz body formation, cyanosis and tissue necrosis in humans [25].

2. Experimental

2.1. Reagents

Methylene blue dye (98% ≤ purity) was obtained from Ciba Ltd. and was used without further purification using bi-distilled water. Its structure contain secondary amine group. Titanium dioxide (TiO_2) from Ti-oxide International Ltd., London (Rutile Type-Purity 99% SP.gr. 4.05-Grade R–CR_2) was utilized as a photocatalyst. Ammonium sulfate was used as sulphation source where ammonium metavanadate was used as a source of vanadium and they were A.R. grade. Degussa P25 consists of 75% anatase and 25% rutile with a specific BET-surface area of 50 $m^2\ g^{-1}$ and primary particle size of 20 nm was used for comparison purposes.

2.2. Catalyst modification

2.2.1. Preparation of $2V_2O_5/TiO_2$

Loading of V_2O_5 on TiO_2 support was performed via incipient wetness impregnation technique. A solution of 0.1378 g of NH_4VO_3 (2 wt.% V_2O_5) was vigorously stirred with small amounts of oxalic acid to improve its dissolution (in a ratio NH_4VO_3/oxalic acid = 0.5 M). The solution was slowly added to 3 g of TiO_2 with stirring at 353 K for 2 h. Oxalic acid solution was evaporated at 383 K, dried at 393 K for 1 h and then calcined at 773 K for 6 h in an air oven.

The color after calcinations was yellow.

2.2.2. Preparation of $2V_2O_5/TiO_2$–SO_4

Anchoring sulfate groups on/in titania sample was done by adding a definite amount of dissolved $(NH_4)_2SO_4$; to achieve 5 wt.% SO_4 on TiO_2 support. The slurry was stirred for 2 h, drying at 393 K, and then calcined at 773 K for 6 h. Vanadium containing sulfated titania sample was prepared as exactly mentioned above.

The color after calcinations at 773 K for 6 h was dark yellow.

2.3. Photoreactor and experimental procedure

The UV source is a 100 W Hg lamp (output mainly at 400 nm, Toshiba SHLS-1002 A) that placed 25 cm on the top of the batch photoreactor. It should be mentioned that an appropriate cut-off filter is placed to completely remove wavelengths shorter than 400 nm and to ensure that irradiation was achieved by visible light wavelengths only. The light intensity was estimated to be approximately 125 W m^{-2} from the light source incident to the top of the Pyrex beaker with the total volume of 500 ml. The UV-irradiated photoreactor was placed on a magnetic stirrer to ensure homogenous mixing during irradiation.

A general photocatalytic procedure was carried out as follows: 0.1 g of catalyst was suspended in a fresh aqueous dye solution ($C_0 = 0.05\ g\ l^{-1}$, 100 ml). The suspension was stirred in the dark for 35 min to ensure establishment of adsorption–desorption equilibrium of MB dye. Prior exposing the suspension to UV-irradiation sorption kinetics experiments was determined. Samples were withdrawn from a sample point at certain time intervals and analyzed for decolorization and degradation of methylene blue dye. Decolorization of dye solutions and aromatic ring destruction were checked and controlled by measuring the absorbances of dye solutions at different intervals using a UV–vis Shimadzu 2101-PC Spectrophotometer.

The maximum absorbance of the dye was at 664 nm that taken as a way for following up the MB degradation. A pH-meter (Hach) was utilized for the adjustion and investigation of pH variation during the process. The pH of the dye solutions was adjusted prior to irradiation by NaOH or H_2SO_4 to be at six.

2.4. Characterization

The X-ray diffractograms of various titania samples were measured by using a Philips diffractometer (type PW 3710). The patterns were run with Ni-filtered copper radiation ($\lambda = 1.5404$ Å) at 30 kV and 10 m A with a scanning speed of $2\theta = 2.5^\circ\ min^{-1}$. The crystallinity of the prepared samples was calculated using the ratio of the sum of the areas of the most intense peaks for modified TiO_2 samples to that of the same peaks for the standard TiO_2 rutile and multiplying by 100. Rietveld method, which permits the reproduction of the whole diffractogram through the optimization of both structural (peak

position and intensity) and non-structural (peak shape) data is used to evaluate the determination of cell parameters and volume increase due to insertion of guest ions in the titania structure.

Dynamic light scattering, LB-500, was used for determining particles size. Sample preparation was carried out as follows: dispersion of 20 mg of the sample in H_2O together with sodium hexametaphosphate was stirred for 10 min. The suspension was ultrasonicated for 10 min then acquired for measurement.

FT-IR spectra of the samples were recorded with a JASCO single beam FT-IR 5300-spectrometer with 50 co-added scans at 2 cm^{-1} resolution. All IR measurements were carried out at room temperature using KBr technique.

UV–vis absorption spectra of the materials were obtained for the dry pressed disk samples using UV–vis spectrophotometer (Shimadzu 2101-PC) between 190 and 750 nm range. Absorption spectra were referenced to $BaSO_4$.

The nitrogen adsorption isotherms were measured at 77 K using a conventional volumetric apparatus. The specific surface area was obtained using the BET method. The micropore volume and the external surface area were obtained from the *t*-plot method.

Thin, but intact, self-supporting wafers (30 ± 5 mg cm^{-2}) of the adsorbents were prepared and mounted inside a specially designed, heatable and evacuable, all quartz glass IR cell. The cell containing samples, equipped with CaF_2 windows, was hooked to a pyrex glass Gas/Vac handling system and evacuated to 10^{-5} Torr at 523 K prior subjecting to 8 Torr portion of pyridine vapor that was expanded at 300 K at which adsorption of Py takes place. A spectrum of the gas phase was recorded before a 5 min degassing of the cell (at 300 K) and taking a spectrum of the wafer plus irreversibly adsorbed pyridine. By absorption subtraction of the cell and wafer, IR difference spectra of the gas phase and Py adsorbed species were obtained, respectively.

TOC (total organic carbon) analysis was conducted using a Dohrmann DC-180 carbon analyzer, which employs the low temperature UV/persulfate oxidation method [26]. Filtered samples (using PTFE syringe filters) were stored in 5 ml sample vials sealed with septa, to allow measurement of dissolved inorganic carbon, without CO_2 diffusing into or out of the sample prior to analysis.

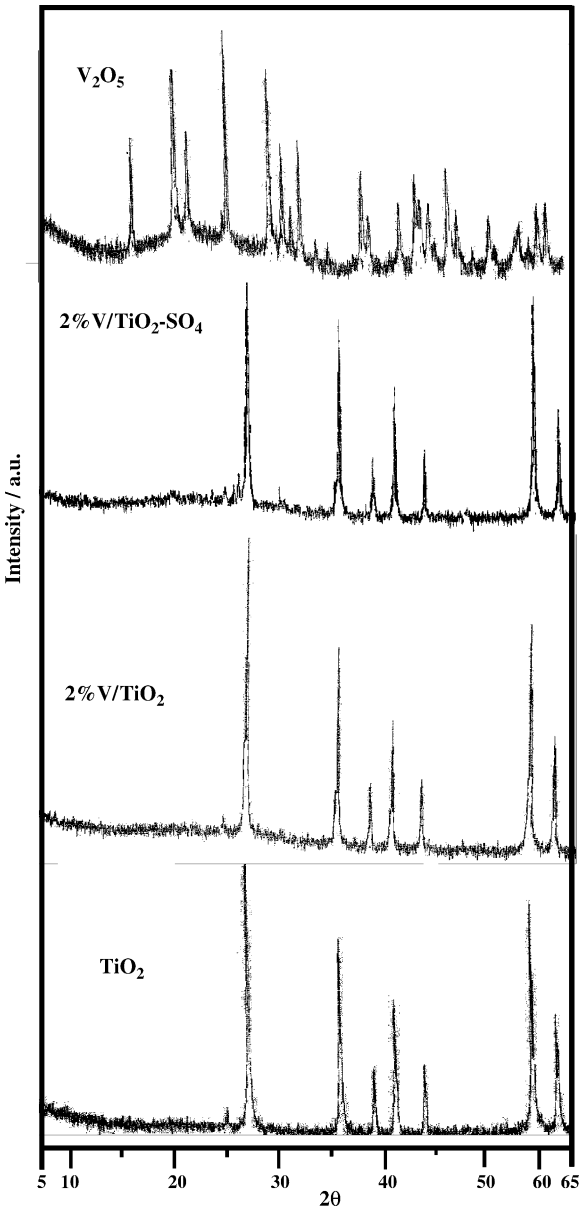

Fig. 1. XRD patterns of rutile TiO_2, 2V/TiO_2 and 2V/TiO_2–SO_4 in comparison with V_2O_5.

3. Results and discussion

3.1. Structural analysis of the catalysts

3.1.1. XRD and crystallites size

Fig. 1 shows that the patterns of 2V/TiO_2 and 2V/TiO_2–SO_4 have uniform rutile structures similar to those of the parent rutile TiO_2, which exposed reflections at *d*-spacings 3.25 (110), 2.99 (200), 2.49 (101), 2.19 (111), 2.05 (210), 1.69 (211) and 1.62 (220) [27]. The crystallinity percentage of 2V/TiO_2 measures 96% from the TiO_2 sample that taken as 100% crystallinity whereas 2V/TiO_2–SO_4 indicates 87% reflecting the effect of sulfation on this particular sample, i.e. mutual interaction between TiO_2 and SO_4 moieties. The values of full-width-at-half maximum (FWHM) of the (110) peak was not much different for all titania samples except V/TiO_2–SO_4 that showed little widening and hence possesses smaller crystallites size, comparatively. There is no V_2O_5 species were developed for vanadium containing samples probably for their high dispersion at such low loadings in both samples and/or for decreasing the crystallites size of V_2O_5 to be detected by XRD technique ($\leq$2 nm). Anatase phase was not observed for all samples even following V incorporation.

The data refined using full prof-98 program showed a good agreement between calculated and observed patterns. The lattice parameter *a* for TiO_2 material measured a value equal 3.7562 Å where TiO_2–SO_4 indicated a value comprise of 3.7991 Å reflecting the incorporation of SO_4 in the structural lattice of TiO_2. The lattice parameter *a* increased to 3.9220 and 3.810 Å following V incorporation into TiO_2–SO_4 and TiO_2 showing the well incorporation of V ions in the former achieving higher expansion comparatively. Values of the cell volume of the various

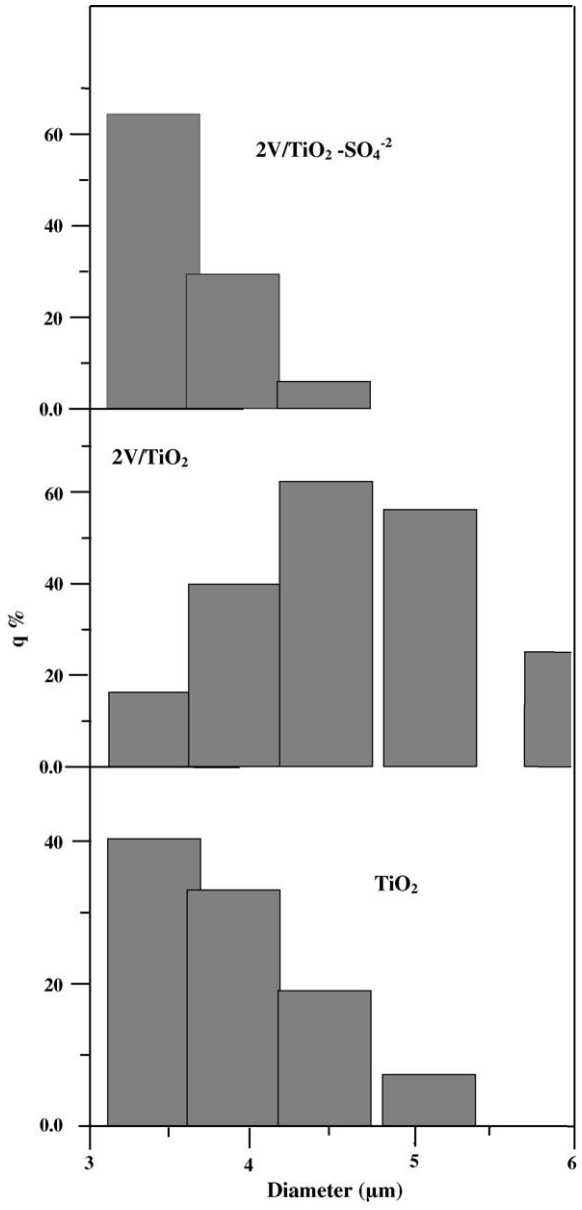

Fig. 2. Particle size distribution of TiO_2, $2V/TiO_2$ and $2V/TiO_2$–SO_4 samples.

titania samples indicate higher value for SO_4 containing sample (6.228 Å^3) when compared with SO_4 free sample (6.178 Å^3) reflecting to some extent the inclusion of SO_4 ions deep inside titania structure.

Fig. 2 gives an idea about the distribution of particles size of all samples illustrating that incorporation of vanadium in TiO_2 ($2V/TiO_2$) exposes particles size at higher dimension from 3.65 μm; in TiO_2, to 4.33 μm; in $2V/TiO_2$. On the contrary, a narrower distribution with a mean particle size 3.39 μm was rendered for $2V/TiO_2$–SO_4 reflecting the role of sulfate groups in exhibiting the finest crystallites size among all samples.

3.2. Surface texturing

The different surface characteristics of the synthesized titania samples were determined and the data obtained is compiled in Table 1. Inspection of this Table reveals the following: (i) the vanadium containing titania samples especially $2V/TiO_2$–SO_4 measured higher surface areas (56.2%) than that of the parent implying the presence of fine particles in this sample as confirmed from XRD and particles size investigations. Thus, the main reason of surface area increment is due to the retardation of crystallization of the TiO_2 following the sulfation process. This lowering degree of crystallinity, as evidenced from XRD pattern, supports the increase in surface area via sulfate treatment. In addition, this sample has the highest microporous surface and volume among all samples, confirming that it preserves higher microporous characteristics (microporous volume and internal surface); (ii) the values of external surface area of the various samples comprise values > 10% of the S_{BET}, indicating the porous nature of these materials where that of $2V/TiO_2$ measured a value comprises 44.8%. This indicates that the latter sample posses appreciable mesoporosity as conceived from microporosity percentages that measured 48%, i.e. the percentage mesoporosity is 52% (prevailing mesoporosity); (iii) the computed values of pore radius of different samples show the dominant of mesoporosity (27–43 Å). The sample designated as $2V/TiO_2$ measured maximum V_p^{total} and maximum r when compared with rest of samples indicating the enforced location of V species in the pores of this sample leading to an effective pore widening and pore volume. Additionally, this sample measured the highest V_p of wide pores (0.2113 cm^3 g^{-1}) between all samples giving a criterion on increasing the diffusion of vanadium ions into the pores of titanium sample.

$V_{l–t}$ plots of the samples (Fig. 3), those constructed depending on the value of C-constant in the BET equation; indicate intracrystalline mesopores as illustrated from upward deviations depicted for all samples. The $V_{l–t}$ plots obtained for $2V/TiO_2$ and $2V/TiO_2$–SO_4 samples show larger upward deviations (as noted in the t range 6–12.5 and 4–12.5 Å, respectively) when compared with that of the parent TiO_2 sample (t = 5.5–11 Å) proposing wider pore radius and pore volume. Comparable swings or hysteresis loops were observed in adsorption–desorption isotherms

Table 1
Texturing properties of V contaning sulphated and non-sulphated titania catalysts

Samples	S_{BET} (m^2/g)	S_t (m^2/g)	S^{ext} (m^2/g)	S^{μ} (m^2/g)	S^{meso} (m^2/g)	V_p^{total} (cm^3/g)	Vp^{μ} (cm^3/g)	V_p^{meso} (cm^3/g)	r$^-$ (Å)	Microporosity (%)
TiO_2	220	234	28	68	20	0.2382	0.1829	0.0553	27.1	77
$2V/TiO_2$	234	287	105	44	49	0.4022	0.1910	0.2113	43.0	48
$2V/TiO_2$ –SO_4^{-2}	345	314	47	104	34	0.3759	0.2841	0.0919	27.2	76

Note: BET-surface area (S_{BET}); surface area derived from $V_{l–t}$ plots (S_t); external surface area (S^{ext}); surface area of micropores (S^{μ}); surface area of wide pores (S^{meso}); total pore volume $\left(V_p^{total}\right)$; volume of micropores (Vp^{μ}); volume of wide pores $\left(V_p^{total}\right)$; mean pore radius (r^-); microporosity percentages. Vp^{μ}/V_p^{total}.

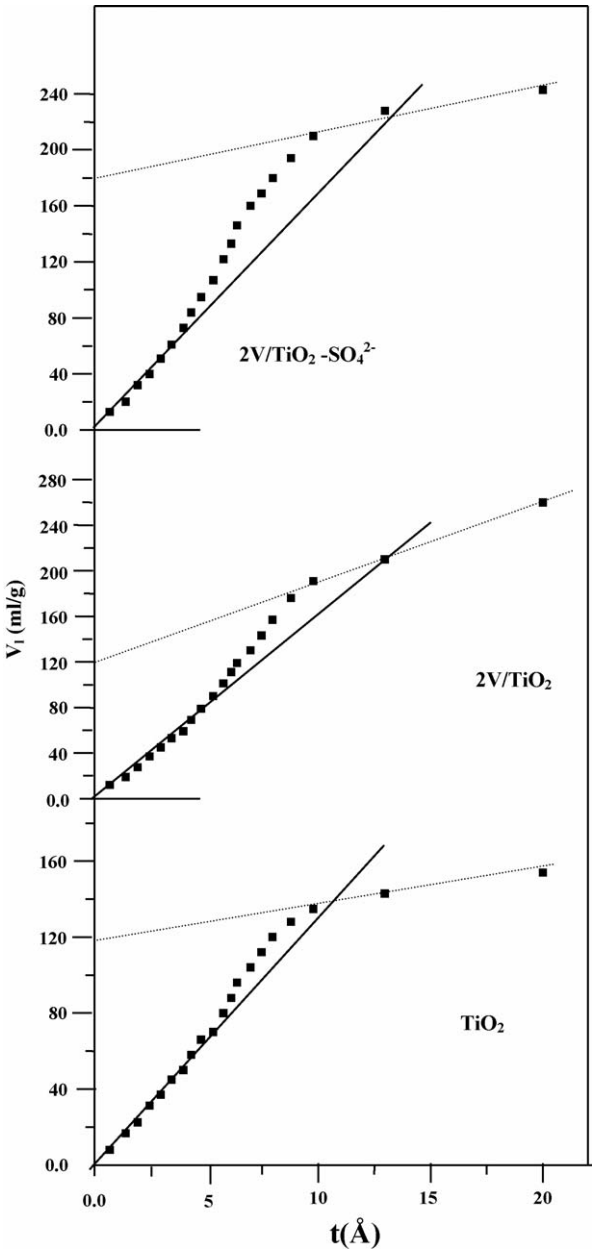

Fig. 3. V_{l-t} plots of TiO_2, $2V/TiO_2$ and $2V/TiO_2$–SO_4 samples.

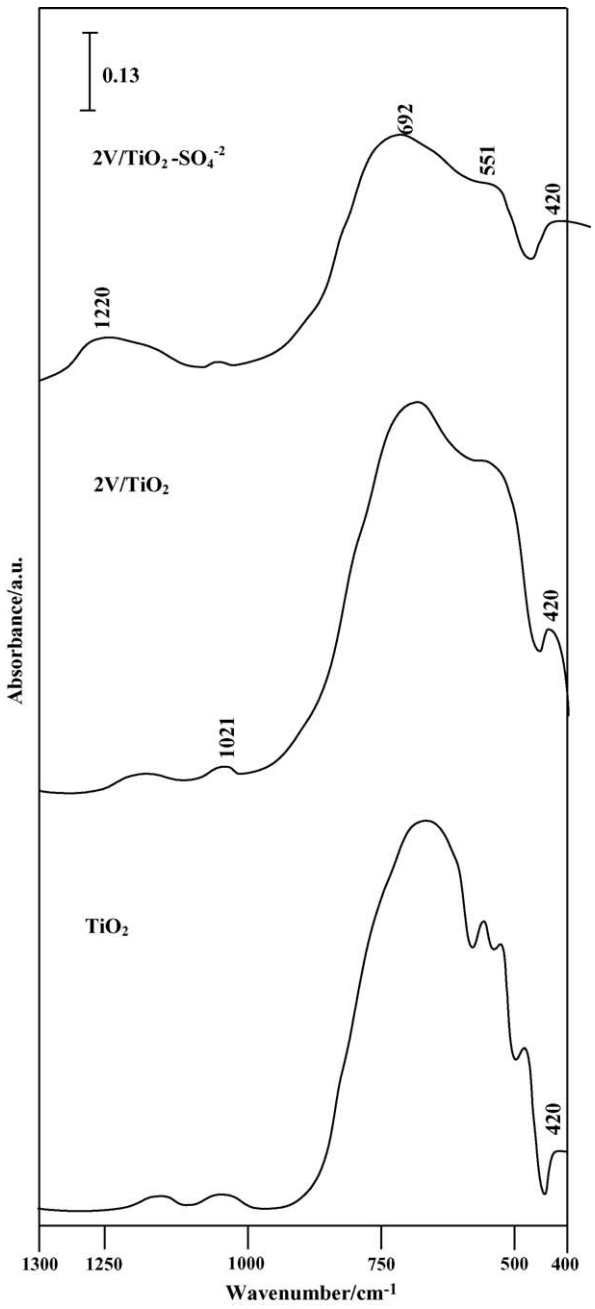

Fig. 4. FT-IR spectra of TiO_2, $2V/TiO_2$ and $2V/TiO_2$–SO_4 in the 400–1300 cm^{-1} range.

of type IV (not shown) for former samples at relative pressures p/p^0 0.45–0.9 and 0.4–0.9, respectively, indicating the presence of mesopores. A sharp adsorption step at p/p^0 near 0.35 is observed for all samples due to capillary condensation in mesopores.

3.3. IR spectroscopy

Fig. 4 shows the FT-IR spectra of vanadium containing titania samples in addition to that of the parent TiO_2 in the frequency range of 400–1300 cm^{-1}. The latter sample shows bands at 420, 475, (557, 539 doublet) and 640 cm^{-1} indicative of the rutile phase of TiO_2 and characteristic of bending vibration of Ti–O bonds [28]. In addition, two bands at 1050 and 1153 cm^{-1} originated from surface vibrations incorporating water molecules causing deformation of the surface TiO_6 octahedrons of surface Ti atoms [29]. For $2V/TiO_2$, bands at 420, 551 and 681 cm^{-1} are depicted in addition to a small band at 1021 cm^{-1} apart from that seen at 1050 cm^{-1}. However, the doublet bands seen in TiO_2 were disappeared in $2V/TiO_2$. It appears that inclusion of vanadium ions modified the spectrum obtained for TiO_2 in doing some changes such as shifting the band at 640 cm^{-1} into 681 cm^{-1} and the appearance of the single band at 551 cm^{-1} in $2V/TiO_2$ instead of the doublet seen at 557 and 539 cm^{-1} in TiO_2. This indeed proposes that a strong interaction is devoted between vanadia and titania particles. The weak band at 1021 cm^{-1} is indicative for the presence of isolated

monovanadate species [30]. Vanishing the band at 475 cm^{-1} in TiO_2 spectrum due to Ti–O–Ti is probably indicative for the selectivity of *V* ions to such type of stretching vibrations.

The spectrum of $2V/TiO_2$–SO_4 preserved the same bands revealed for $2V/TiO_2$ except marked decrease in intensities for the bands at 551, 681 (692) cm^{-1} and 1021 cm^{-1} reflecting some evidence for the strong interaction between sulfate groups and titania particles and indicates as well a decrease in crystallinity following sulfation, as emphasized previously using XRD investigations. The decrease in intensity of the monovanadate band at 1021 cm^{-1}; associated with V–O, could be due to migration of vanadium ions into the TiO_2–SO_4 vacant positions but more extensive tests are required to prove this definitively. The band at 551 cm^{-1} that recognized as distinct band in $2V/TiO_2$ shown as a shoulder in $2V/TiO_2$–SO_4 signifying its sensitivity towards SO_4 ions. This spectrum shows a broad band at 1220 cm^{-1} ascribed to the asymmetric stretching mode of S–O linkages [31] and verifying the involvement of it in the titania structure. From the foregoing results of XRD, particles size, texturing and IR, one can conclude the presence of SO_4^{2-} in the lattice of Ti atoms probably in S^{4+} structure substituting for some of the lattice Ti atoms. This was in harmony with the work of T. Ohno et al. [32] who prepared and characterized S-doped TiO_2 (anatase) and they suggested that the oxidation state of S is determined to be mainly S^{4+} from XPS investigations.

3.4. UV–vis absorption spectra

The optical absorption spectra of the materials are shown in Fig. 5. The neat TiO_2 sample shows a single peak at 245 nm while TiO_2–SO_4 shows three optical absorption peaks at 250, 410 and 470 nm reflecting a distortion occurred in TiO_2 species. V/TiO_2–SO_4, on the other hand, shows peaks at 200, 275 and 430 nm indicating probably the presence of bulk vanadium oxide particles (430 nm).

Commercial Degussa P-25 TiO_2 used to show a single peak at 400 nm; which corresponds to a band gap energy of 3.1 eV [33], while TiO_2–SO_4 that shows an extra peak at 470 nm corresponding to the band gap energy of 2.66 eV manifests higher absorption of solar energy. It has been acknowledged that solar wavelength shows maximum irradiance at the wavelength region of 450–480 nm [33]. Since TiO_2–SO_4 band gap corresponds to this region, it can absorb relatively higher photon flux compared to TiO_2 Degussa. The irradiances corresponding to the wavelengths of 410 and 470 nm are 1.59 and 1.962 W m^{-2} nm^{-1}, respectively. V/TiO_2 shows peaks at 275, 375 and 410 nm. The presence of bands at 375 and 410 nm refers to octahedral V species probably having two different structures. Similar bands were seen in V containing silica based microporous materials and associated with distorted tetrahedral V^{5+} species [34]. The shift of the charge transfer bands; from 245 nm in TiO_2, to high frequencies; in V/TiO_2 (275 nm) and V/TiO_2–SO_4 (275 nm) exceeding that of TiO_2–SO_4 (250 nm) indicate a distortion in tetrahedral Ti species as a result of V insertion. It should be mentioned that the latter material showed stronger red shift than V/TiO_2–SO_4 that owned lower intense yellow color, comparatively.

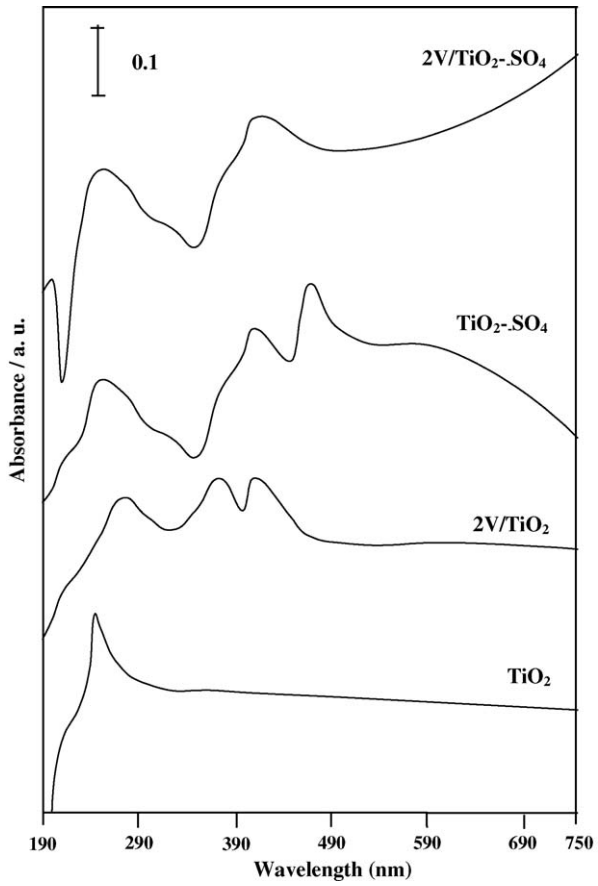

Fig. 5. UV–vis absorption spectra of TiO_2, TiO_2–SO_4, $2V/TiO_2$ and $2V/TiO_2$–SO_4.

3.5. Acidity evaluation

Fig. 6 compares νCCN spectra of Py adsorbed on V/TiO_2 and V/TiO_2–SO_4 taken following outgassing at 300 K. The spectrum of $Py/V/TiO_2$ at 300 K displays a band structure the strongest features of which are indicative of formation of Lewis Pyridine (LPY) species, i.e. bands at 1456, 1470 and 1600 cm^{-1}. The display of a strong band at 1540 cm^{-1} due to Bronsted pyri-

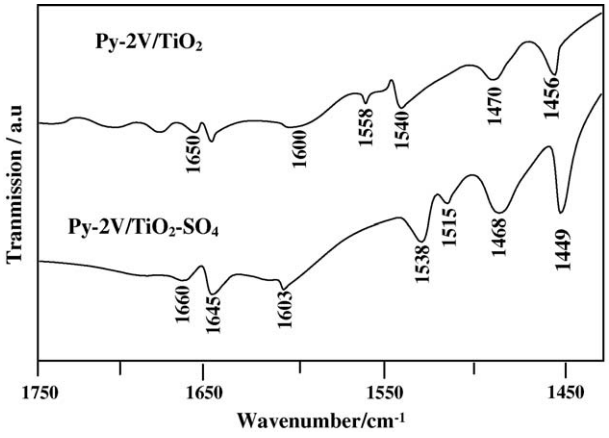

Fig. 6. In situ FT-IR spectra in the 1400–1750 cm^{-1} range due to pyridine adsorption at room temperature. The spectra were recorded after evacuation for 10 min at 300 K.

dine (BPY) let us assigns the ones at 1645 and 1650 cm^{-1} to same species but probably accounted for the involvement of two different types Bronsted acid sites. The existence of a band at 1558 cm^{-1} is indicative for oxidative break down of LPY species into carbonaceous surface species; at such low temperature (300 K), implying the existence of considerably reactive basic sites. The latter result is confirmed also through the exposed band at 1680 cm^{-1} ascribed to νC=O of α-pyridone species. That band is freed from the contribution of δOH absorption of surface water molecules as evidenced from the permanent existence of the band even following evacuation at 473 K (not shown).

On V/TiO_2–SO_4, Py adsorption at 300 K is shown to lead to formation of higher density LPy species comparatively, i.e. 1449, 1468 and 1603 cm^{-1} as well as BPy ones, i.e. bands at 1538, 1645 and 1660 cm^{-1}. Moreover, a medium band at 1515 cm^{-1} indicative of pyridinum oxide species is also depicted as previously envisaged by others [35]. These results have been considered [36] indicative of existence of reactive basic O_2^- species on V/TiO_2–SO_4 surfaces but of lower density than those delivered on $2V/TiO_2$. Generally, the detection of pyridinium oxide species is rather indicative of the availability of acid base pair sites. The higher the frequency assumed by the ν19b mode (1456 cm^{-1}) for $2V/TiO_2$, the stronger the acidity of the Lewis coordination site. Hence, the formation of Py oxidation species seems to have been preceded by conversion into α-pyridone species (νC=O band at 1680 cm^{-1}) and hence reveals existence of active nucleophilic (basic) OH groups rather than V/TiO_2–SO_4. It can be inferred that differences in reactivity of basic sites are related to the sulfate moieties, that affect the geometric arrangement of OH^- or/and O_2^- ligands. This explains the reactivity of basic sites of V/TiO_2 due to the major contribution of LPY species comparatively. This figure also shows that Bronsted acid sites, i.e. proton acidity, appeared on the sulfated sample with higher population than that on non-sulfated one.

3.6. Methylene blue degradation

3.6.1. Activity

The degradation of MB as a model reaction was studied to investigate the photocatalytic activities of $2V/TiO_2$ and $2V/TiO_2$–SO_4 samples under UV irradiation. The changes in the concentration of MB recorded during UV irradiation at specific time intervals are shown in Fig. 7. Control experiment shows that MB is not degraded in the dark or under UV light in the absence of catalysts for 1.5 h. It can be seen that the conversion of MB was higher when UV-light irradiation was applied in the presence of $2V/TiO_2$–SO_4, i.e. the conversion of MB reached 98% after 75 min UV-light irradiation. On the other hand, the V/TiO_2 catalyst shows a conversion activity approaches 78% in the same time. These results indicate the superior photocatalytic activity of V/TiO_2–SO_4 when compared with V/TiO_2, suggesting that the degradation of MB originated not only from V/TiO_2 but also from sulfate containing catalyst.

The degradation of MB on the neat TiO_2 and Degussa P-25 (not shown) indicated, respectively, 60% and 70% decrease in the concentration. Unexpectedly, TiO_2–SO_4 indicates a conversion comprises of 73% relatively similar to that committed for Degussa. This demonstrates the higher solar photocatalytic activity of V/TiO_2–SO_4 under similar conditions. This can be rationalized to surface and structural characteristics that indicated large surface area, mesoporous texture and high crystallinity besides indeed to the exhibited decrease in band-gap energy. Degradation of MB via photocatalysis of rutile TiO_2 modified with polycarbonate and polymethyl methacrylate indicated activities in the range 80–90% [37].

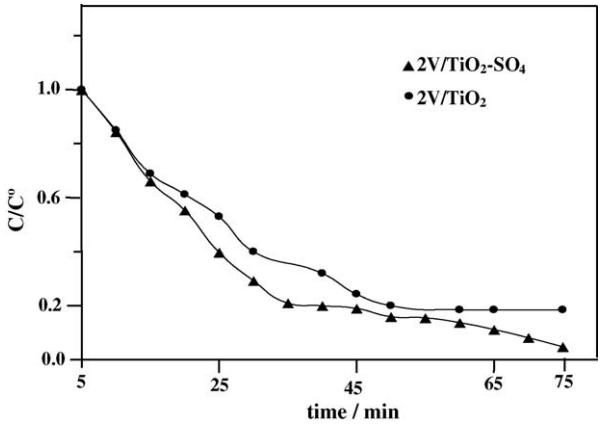

Fig. 7. Concentration of MB changes as a function of UV-irradiation time. Conditions; $C_0 = 0.05$ g/l, weight of catalyst 0.1 g, $V = 100$ ml.

In a way of searching on the reasons responsible for increasing the decolor rate of MB on sulfated titania, the adsorption course of all TiO_2 samples; under dark conditions, was carried out. The amount of MB removed from the liquid phase containing sulfated titania sample was increased by time reaching to 28% and stabilized after 30 min. On the other hand, the TiO_2 parent sample showed negligible adsorption ability whereas, $2V/TiO_2$ induces a removal percentage comprises of 23% and stabilized after 15 min. The slight increase in MB amount adsorbed on $2V/TiO_2$–SO_4 could be due to increasing the mesopore radius of the latter (43.0 Å) that was able to incorporate MB (15.0 Å) molecules, i.e. MB molecules can diffuse freely inside the pores. This implies that increasing the pore radius intensively is not the only factor responsible for effective adsorption of MB but also the S_{BET} value that showed an incredible enhancement in $2V/TiO_2$–SO_4.

Another driving force for the adsorption process is the increased concentration gradient between the dye in solution and on the sulfated titania sample. Considering the dye adsorption is the prime factor affecting the photocatalytic activity thus, the difference in the MB removal between the UV illuminated and dark conditions (Δ(UV dark)) is used as an apparent measure to evaluate only the impact of the UV illumination on the MB removal. This indicates that the activity revealed upon exposing to UV irradiation for $2V/TiO_2$–SO_4 ($98 - 28 = 70\%$) is indicative of existing higher photodecomposition sites on its surface.

In general, external mass transfer is characterized by the initial solute uptake and can be calculated from the slope of plot of C/C_0 versus time. The slope of such plots (especially in the first 10 min) can be calculated by either assuming a polynomial relation between C_t/C_0 and time or assuming that the relationship

is linear for the first points collected in 10 min. These methods were used by Fernadez et al. [38] while studying the adsorption of lauryl benzyl sulfonate on algae residue. The second method was employed in our case and the calculated sorption K_s was found to be 0.0176 and 0.01699 min^{-1} for $V/TiO_2–SO_4$ and V/TiO_2 catalysts, respectively, assuming that the external mass transfer occurs in the first 10 min for both catalysts in addition to the increased rate on the former, comparatively.

To check whether S_{BET} of $2V/TiO_2–SO_4$ is effective or not in the process of MB oxidation, a pre-calcination at 973 K for the sample was carried out and hence a decrease in surface area was attained (242 $m^2\ g^{-1}$; 30% loss). This sample showed a decrease in conversion comprised of 75%, in the same time. The activity variation with rise of calcinations temperature could be due to loss of surface area in addition to expected loss in SO_4 amounts; then there were less active centers, as has been shown for $SO_4/Zr–Fe–Si–O$ catalyst whilst esterification of acetic acid and butanol that showed a decrease in activity following calcinations at high temperatures [39].

3.6.2. Kinetics

The investigation of MB kinetics in aqueous solution under UV-light irradiation is shown in Fig. 8. The degradations follow an apparent first order process. Assuming that the hydroxyl radical OH is the primary oxidant for degradation of MB, a chemical kinetics for the process may be written as

$$OH + MB \rightarrow \text{products} \quad (1)$$

That allows an expression for the reaction rate of the degradation of MB, such as

$$r = \frac{dc}{dt} = \frac{kKC}{1 + KC} \quad (2)$$

where r is the degradation rate of the reactant (mg/l min), C the concentration of the reactant (mg/l), t the illumination time, k the reaction rate constant and K is the adsorption coefficient of the reactant (l/mg). When the chemical concentration C_0 is micromolar, Eq. (2) can be simplified to an apparent first-order equation:

$$\ln\left(\frac{C_0}{C}\right) = kKt = K_{app} \quad (3)$$

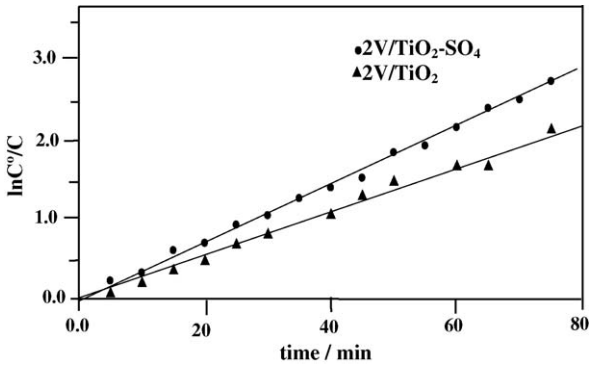

Fig. 8. First-order relation $\ln(C_0/C) = F(t)$. Conditions; $C_0 = 0.05$ g/l, weight of catalyst 0.1 g, $V = 100$ ml.

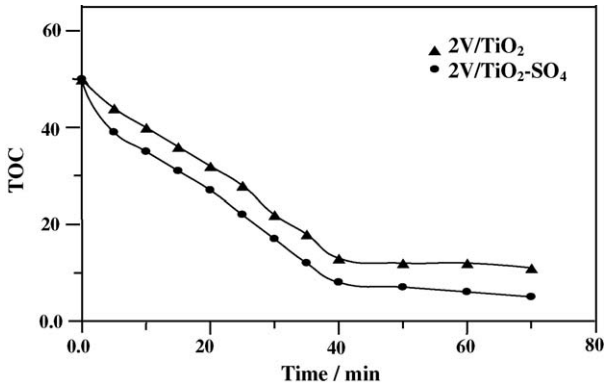

Fig. 9. Mineralization of 0.2 mM MB in the presence of UV irradiation in presence of 0.1 g catalyst.

A plot of $\ln(C_0/C)$ against time represents approximately linear straight lines, showing the case of the first-order reaction. The slope of the line equals the apparent first-order rate constant K_{app}. As can be seen from the figure, the degradation rate is faster for $2V/TiO_2–SO_4$ than for $2V/TiO_2$. The determined K_{app} values are 0.037 min^{-1} for the former and 0.030 min^{-1} for the latter.

3.6.3. TOC measurement

Changes in the TOC of the suspensions reflect the degree to which the dye has been degraded or specifically mineralized during irradiation. The results of TOC measurements under UV irradiation show values comprise of 92% and 78% within 75 min for $2V/TiO_2–SO_4$ and $2V/TiO_2$ samples (Fig. 9), respectively. Since a greater TOC decay is found for $2V/TiO_2–SO_4$ than for $2V/TiO_2$, it is apparent that $OH^{\cdot}$ is more efficiently generated on the former than that on the latter.

The dependence of the photodecomposition on the sulfate groups attached to Ti can be explained in view of increasing the electron accepting capacity as envisaged from increasing the Lewis acid sites density and thus a decreased in the recombination of holes and electrons is expected, i.e. long-lived OH radicals. Small particles of $2V/TiO_2–SO_4$ on the rutile surface act as strong catalyst by themselves because of their highly active surfaces. Implanting SO_4 groups and their occupying lattice sites in rutile, could create impurities level results between the energy band gap rutile [40–41] to contribute to decreasing photoenergy to be susceptible for activation.

Generally, one can attribute the improvement of the photocatalytic activity of metal incorporated titania; only at such low loadings, when compared with the neat titania to the increased electronegativity of V ions thus behave as an electron acceptor centers to decrease any possible recombination between holes and electrons [42]. Another possibility of degradation of MB can be obtained through the existed reactive basic sites (O_2^-) detected on the surface of sulfated titania. This can be attained by reacting the produced oxygen with photogenerated electron (e^-) leading to the generation of $O_2^{\bullet -}$ and thus preventing the recombination of e^- and h^+. $O_2^{\bullet -}$ also can degrade MB as reactive oxygen species [43]. However, it seems that $O_2^{\bullet -}$ is not the only active species capable for degrading MB since V/TiO_2 owns larger amounts of such species, comparatively. This let us pre-

sume that hydroxyl radical is considered as the main oxidizing agent. On the other hand, the probability of yielded $O_2^{\bullet -}$ to react with H protons, specifically V/TiO_2–SO_4, to produce $HO_2^{\bullet}$ is most likely since sulfated titania acquired higher Bronsted acidity and thus $HO_2^{\bullet}$ is one of the oxidizing agents present in the reaction mixture but however of lower activity when compared with $OH^{\bullet}$.

Generally, the revealed photocatalytic activity of V/TiO_2–SO_4 upon UV irradiation is most probably due to charge-transfer excited state between V species and TiO_2 particles. An electron transfer from O_2^- to V^{5+} ions can develop $(V^{4+}–O^-)^*$ moieties, which by their turn can play a role in the enhancement of the reaction as well. This was envisaged previously whilst photocatalytic reduction of NO by hydrocarbons over VS-1 catalysts [44].

4. Conclusions

The modification of rutile-V/TiO_2 by sulfate ions contributes to promote the photocatalytic efficiency of rutile towards fully decomposing MB dye in 70 min reaction time; in presence UV lamp emitting at 400 nm, when compared with sulfate free titania sample. The physicochemical properties of sulfated V/TiO_2 that were characterized by XRD, FT-IR, UV–vis, N_2 adsorption, particles size and Pyridine-FT-IR indicated that the promotional effect of sulfated sample was due to the high surface area, mesopore structures, small crystallites size, decreased band-gap energy and appropriate basic (OH^-, O_2^-) sites in addition to the substantial amounts of Lewis acidity that owned vacant sites susceptible for more active sites. The role of sulphate and vanadium in promoting the degradation of MB was well followed and investigated. Degradation of MB was 1.4 times lower on Degussa P-25 compared to V/TiO_2–SO_4.The sorption process was found to be dependent mainly on external transfers at earlier stages and hence high lighting the effect of surface properties on the adsorption process and consequently on the catalytic enhancement. Lowering the red shift of V/TiO_2–SO_4 than TiO_2–SO_4 highlighted the importance of structural and surface properties; besides the band gap energy, of the former in exhibiting higher photocatalytic activities.

Acknowledgment

The authors would like to express their appreciation and thanks to Saudi Arabia Basic Industrial Company (SABIC) for their finacial support and help during carrying out this reaserch work.

References

[1] H.M. Pinheiro, E. Touraud, O. Thomas, Dyes Pigments 61 (2004) 121.
[2] K.T. Chung, G.E. Fulk, A.W. Andres, Appl. Environ. Microbiol. 42 (1981) 641.
[3] T. Sauer, G. Cesconeto Neto, H.J. Jose, R.F.P.M. Moreira, J. Photochem. Photobiol. A: Chem. 149 (2002) 147.
[4] C.M. So, M.Y. Cheng, J.C. Yu, P.K. Wong, Chemosphere 46 (2002) 905.
[5] I. Sopyan, M. Watanabe, S. Murasawa, K. Hashimoto, A. Fujishima, Chem. Lett. (1996) 69.
[6] M.M. Mohamed, Appl. Catal. A 267 (2004) 135;
V. Štengl, J. Šubrt, Způsob výroby fotokatalyticky aktivní titanové běloby, PV 2000–2814 (The way of production of photocatalytically active titanium white, Czech patent).
[7] K. Nagaveni, G. Sivalingam, M.S. Hegde, G. Madras, Appl. Catal. B 48 (2004) 83.
[8] L.V. Malysheva, E.A. Paukshits, K.G. Ione, Catal. Rev. Sci. Eng. 37 (1995) 179.
[9] L.E. Bertea, H.E. Kouwenhoven, R. Prins, Appl. Catal. A 129 (1995) 229.
[10] M.M. Mohamed, T.M. Salama, T. Yamaguchi, Colloids Surf. 207 (1–3) (2002) 25.
[11] E. Suzuki, K. Tohmori, Y. Ono, Chem. Lett. (1987) 2273.
[12] O.L. Wright, J. Teipel, D. Thoennes, J. Org. Chem. 30 (1965) 1301.
[13] P. Laszlo, J. Vandormeal, Chem. Lett. (1988) 1843.
[14] M. Hino, K. Arata, J. Chem. Soc., Chem. Commun. (1995) 53.
[15] H. Matsuhashi, T. Tanaka, K. Arata, J. Phys. Chem. B 105 (2001) 969.
[16] K. Arata, H. Matsuhashi, M. Hino, H. Nakamura, Catal. Today 81 (2003) 17.
[17] K.T. Wan, C.B. Khouw, M.E. Davis, J. Catal. 158 (1996) 311.
[18] W. Chu, J.P. Hu, F.L. Qiu, Q.L. Chen, Chinese Invention Patent CN [1323] 655A (2001).
[19] (a) M. Hino, K. Arata, Chem. Lett. (1979) 1259;
(b) M. Hino, K. Arata, Chem. Lett. (1979) 477;
(c) M. Hino, K. Arata, J. Chem. Soc., Chem. Commun. (1980) 851.
[20] M.M. Mohamed, B. Abu-Zied, Thermochim. Acta 359 (2) (2000) 109; T. Okuhara, N. Mizuno, M. Misono, Appl. Catal. A: Gen. 222 (2001) 63.
[21] V. Vadivelan, K. Kumar, J. Colloid Interface Sci. 286 (2005) 90.
[22] R. Ashi, T. Morikawa, T. Ohwaki, K. Aoki, Y. Taga, Science 293 (2001) 269.
[23] J.C. Yu, J.G. Yu, W.K. Ho, Z.T. Jiang, L.Z. Zhang, Chem. Mater. 14 (2002) 3803.
[24] W. Choi, A. Termin, M.R. Hoffmann, J. Phys. Chem. 98 (1994) 13669.
[25] K.E. Karakitsou, X.E. Verykios, J. Phys. Chem. 97 (1993) 1184.
[26] Rosemount Analytical, Dohrmann Division, Santa Clara. DC-180 Automated TOC Analyzer Opertation Manual 1989.
[27] C.G. Granqvist, R.A. Buhraman, J. Appl. Phys. 47 (1996) 2200.
[28] T. Lopez, J.A. Moreno, R. Gomez, X. Bokhimi, J.A. Wang, H.Y. Maderia, G. Pecchi, P. Reyes, J. Mater. Chem. 12 (2002) 714.
[29] M.A. Fox, M.T. Dulay, Chem. Rev. 93 (1993) 341.
[30] B. Olthof, A. Khodakov, A.T. Bell, E. Iglesia, J. Phys. Chem. B 104 (2000) 1516.
[31] D. Stoilona, M. Georgiev, D. Marinova, Vib. Spectrosc. 39 (2005) 46.
[32] T. Ohno, M. Akiyoshi, T. Umebayashi, K. Asai, T. Mitsui, M. Matsumura, Appl. Catal: A 265 (2004) 115.
[33] K. Nagaveni, G. Sivalingan, M.S. Hegde, G. Madras, Appl. Catal. B 48 (2004) 83.
[34] S. Dzwigaj, Curr. Opin. Solid State Mater., Sci. 7 (2003) 461.
[35] M.W. Urban, Vibrational Spectroscopy of Molecules and Macromolecules on Surfaces, Wiley, Chichester, 1993, pp. 171–185.
[36] M.I. Zaki, M.A. Hasan, F.A. Al-Sagheer, L. Pasupulety, Colloids Surf. A 190 (2001) 261.
[37] C.-H. Kwon, H. Shin, J.-H. Kim, W.S. Choi, K.H. Yoon, Mater. Chem. Phys. 86 (2004) 78;
M.M. Mohamed, I. Othman, N. Eissa, Microporous Mesoporous Mater. 87 (2005) 93.
[38] N.A. Fernadez, E. Chacin, E. Gutierrez, N. Alastre, Bioresour. Technol. 54 (1995) 111.
[39] H. Tsuji, T. Sagimori, K.-I. Kurita, Y. Gotoh, J. Ishikawa, Surf. Coat. Technol. 158–159 (2002) 208.
[40] W. Chu, J. Hu, Z. Xie, Q. Chen, Catal. Today 90 (2004) 349.
[41] S.-D. Mo, L.B. Nin, D.L. Lin, J. Phys. Chem. Solids 55 (1994) 1309.
[42] K.R. Sunajadevi, S. Sugunan, Catal. Commun. 6 (2005) 611.
[43] Y. Yang, Y. Guo, C. Hu, Y. Wang, E. Wang, Appl. Catal A: Gen. 273 (2004) 201.
[44] M. Anpo, S.G. Zhang, S. Higashimoto, M. Matrioka, H. Yamceshita, Y. Ichihashi, Y. Matsumura, Y. Souma, J. Phys. Chem. B 103 (1994) 9295.